Fluid inclusion evidence for subsurface phase separation and variable fluid mixing regimes beneath the deep-sea PACMANUS hydrothermal field, Manus Basin back arc rift, Papua New Guinea

David A. Vanko,[1] Wolfgang Bach,[2] Stephen Roberts,[3] Christopher J. Yeats,[4] and Steven D. Scott[5]

Received 7 May 2003; revised 9 November 2003; accepted 1 December 2003; published 5 March 2004.

[1] Altered volcanic rocks were cored from over 350 m below the seafloor at the Papua New Guinea-Australia-Canada Manus Basin Hydrothermal Field (PACMANUS) deep-sea hydrothermal field, in the eastern Manus back arc basin. Fluid inclusions in anhydrite veins reveal phase separation and fluid mixing beneath the seafloor. The anhydrite precipitated from high-temperature fluids (150–385°C). At Roman Ruins, a site of active high-temperature venting (220–276°C, measured by submersible), the fluid inclusion thermal depth profile is uniform and high temperature (242–368°C). At Snowcap, a site of warm water effusion (6–65°C), the fluid inclusions indicate high temperatures at depth (270–385°C) but both low and high temperatures in the shallower section. This indicates a flow regime dominated by vertical advection and shallow entrainment and mixing with cool seawater. Inclusions at Snowcap exhibit extreme salinity variations due to phase separation at temperatures above 350°C. Fluids contain Na, Cl, Fe, Zn, Mg, and Ba and a minor gas component such as CO_2 or CH_4. Most inclusions at Roman Ruins exhibit salinities that fall within the range of those observed at modern active vent sites along the mid-ocean ridge system. Fluid inclusion temperatures support a hypothesis, developed previously from Sr-isotopic analysis, that the subseafloor at Snowcap is characterized by mixing between deep-sourced hot hydrothermal fluids and cold seawater-like fluid. Both heating of seawater and cooling of upwelling hydrothermal fluids can be recognized by combining isotopic and fluid inclusion data. In contrast to Snowcap, the regime at Roman Ruins is less varied, with uniformly high-temperature upwelling fluids that have hydrothermally dominated Sr-isotopic ratios. *INDEX TERMS:* 1040 Geochemistry: Isotopic composition/chemistry; 3015 Marine Geology and Geophysics: Heat flow (benthic) and hydrothermal processes; 3035 Marine Geology and Geophysics: Midocean ridge processes; 3665 Mineralogy and Petrology: Mineral occurrences and deposits; 8135 Tectonophysics: Hydrothermal systems (8424); *KEYWORDS:* fluid inclusions, Ocean Drilling Program, anhydrite

Citation: Vanko, D. A., W. Bach, S. Roberts, C. J. Yeats, and S. D. Scott (2004), Fluid inclusion evidence for subsurface phase separation and variable fluid mixing regimes beneath the deep-sea PACMANUS hydrothermal field, Manus Basin back arc rift, Papua New Guinea, *J. Geophys. Res.*, *109*, B03201, doi:10.1029/2003JB002579.

1. Introduction

[2] Numerous discoveries of active high-temperature seafloor hydrothermal systems over the past 25 years, combined with the knowledge gained from petrologic studies of altered fossil systems, have resulted in a first-order understanding of the physical and chemical conditions within the subseafloor regime [e.g., *Alt*, 1995, 1999; *Alt and Teagle*, 2000; *Honnorez et al.*, 1998; *Scott*, 1997; *Von Damm*, 1995]. However, only a few active deep-sea systems have been drilled and sampled in the subsurface, all using technology made available through the Ocean Drilling Program (ODP). These include the TAG hydrothermal field along the basaltic Mid-Atlantic Ridge [*Humphris et al.*, 1995, 1996; *Herzig et al.*, 1998; *Teagle et al.*, 1998; *Tivey et al.*, 1998; *Petersen et al.*, 1998], the sediment-covered Middle Valley and Escanaba Trough areas of the Juan de Fuca Ridge [*Davis et al.*, 1992; *Mottl et al.*, 1994; *Fouquet et al.*, 1998; *Zierenberg et al.*, 1998, 2000], and, with the recent Leg 193 of the ODP, the Papua New

[1]Department of Physics, Astronomy and Geosciences, Towson University, Towson, Maryland, USA.
[2]Department of Marine Chemistry and Geochemistry, Woods Hole Oceanographic Institution, Woods Hole, Massachusetts, USA.
[3]School of Ocean and Earth Science, Southampton Oceanography Centre, University of Southampton, Southampton, UK.
[4]CSIRO Exploration and Mining, North Ryde, New South Wales, Australia.
[5]Department of Geology, University of Toronto, Toronto, Ontario, Canada.

0148-0227/04/2003JB002579$09.00

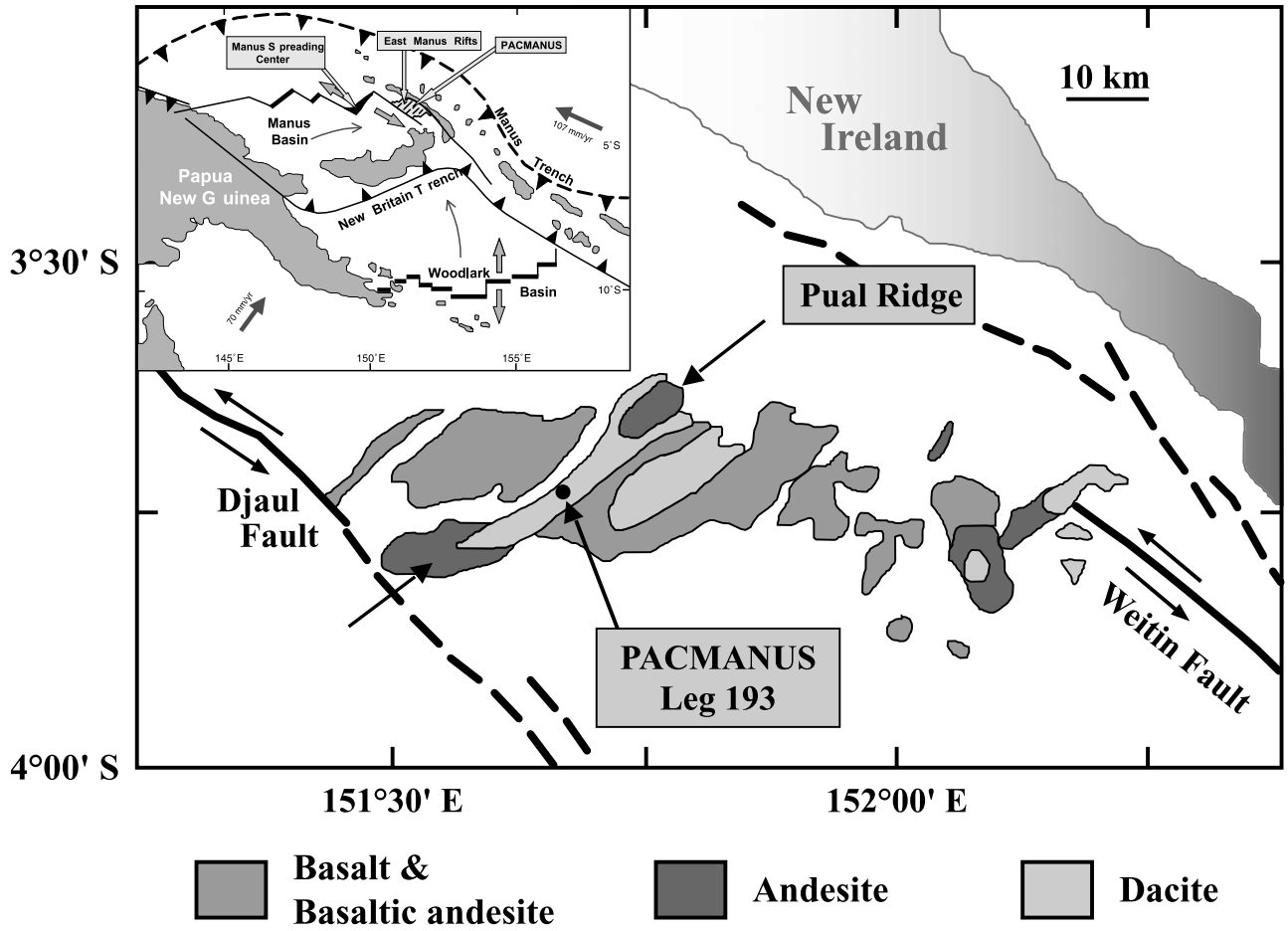

Figure 1. Tectonic setting of the Manus Basin and the location of the PACMANUS hydrothermal field (solid dot), which was the focus of Ocean Drilling Program Leg 193. PACMANUS is on Pual Ridge, whose strike is indicated with two opposing arrows. Modified after *Binns et al.* [2002].

Guinea-Australia-Canada Manus Basin Hydrothermal Field (PACMANUS) hydrothermal field in felsic volcanic rocks of the Manus back arc basin [*Binns et al.*, 2002]. Drilling and coring techniques developed recently for the harsh axial environment provide the means to test assumptions and hypotheses about the subseafloor regime directly.

[3] This paper provides the first direct evidence on subseafloor temperature profiles and fluid compositions in an active felsic-hosted hydrothermal system, using fluid inclusions in vein-filling anhydrite that was sampled at two ODP sites and to depths of up to 350 m below the seafloor (mbsf). The fluid inclusions provide a record of hydrothermal conditions through a significant depth range. This contrasts with studies of active chimneys, which are only sampled directly at the seafloor, and with ODP investigations of fossil systems, where the earlier phases of hydrothermal circulation are overprinted by later waning stages (e.g., DSDP/ODP Hole 504B [*Alt et al.*, 1996; *Gu and Vanko*, 1996]). Furthermore, data for the current paper come from anhydrite veins, which because of the high solubility of anhydrite in cold seawater [*Rimstidt*, 1997], are quite ephemeral and would not be expected to be preserved in older sections.

[4] The present fluid inclusion study concludes that high-temperature hydrothermal fluids with temperatures of 150–385°C precipitated anhydrite beneath the two ODP sites in the PACMANUS field. Subseafloor fluid inclusions from one site (Roman Ruins) are uniformly high-temperature (242–368°C) even to shallow depths, consistent with an advective thermal gradient due to vigorous upflow and vent temperatures of 220–276°C measured at that site [*Auzende et al.*, 1996; *Douville et al.*, 1999; *Ishibashi et al.*, 1996]. Subseafloor inclusions from another site (Snowcap), where present activity involves more gentle warm water effusion, reflect a thermal gradient affected by the entrainment of cool shallow seawater-groundwater. Fluid inclusions vary significantly in salinity and density, a property that is best explained by phase separation of the hydrothermal fluid.

2. Geological Background

[5] The PACMANUS hydrothermal field is located at the crest of Pual Ridge, a 20 km long, 1–1.5 km wide, 500–600 m high volcanic ridge constructed of dacite/rhyodacite volcanic rocks, volcanic breccias, and volcaniclastic sedimentary deposits [*Paulick et al.*, 2004]. On the basis of dredging, the lower parts of Pual Ridge also contain basaltic andesite and andesite. Pual Ridge is situated in the eastern part of the Manus back arc basin north of the New Britain subduction zone (Figure 1) [*Taylor et al.*, 1994]. Back arc

spreading in the central Manus basin involves basaltic volcanism. However, at the eastern end of the Manus Basin, extension is currently occurring between two transform faults in the form of en echelon faulting of and associated volcanism into more siliceous Eocene-Oligocene island arc crust, which was formed when active subduction was directed southwestward along the now extinct Manus subduction zone. The resulting volcanic rocks are more dacitic, with geochemical traits that may reflect crustal assimilation [*Sinton et al.*, 2003] or a genetic relationship with the New Britain arc volcanic rocks (C. J. Yeats, personal communication, 2003).

[6] Prior work in the eastern Manus Basin has demonstrated the presence of several minor and three major hydrothermal fields: PACMANUS; DESMOS, about 23 km to the east; and Susu Knolls, about 40 km east of PACMANUS [*Gamo et al.*, 1997; *Ishibashi et al.*, 1997; *Binns et al.*, 1997]. The PACMANUS field contains several discrete vent sites with active chimneys, iron-oxide mounds, and areas of diffuse venting [*Binns and Scott*, 1993]. Fluid temperatures measured at the orifice of black or gray smokers and clear fluid sulfide chimneys ranged from 220–276°C. The end-member vent fluids exhibited variable salinities, low in situ pH (~3.5), variable and typically high concentrations of H_2S, CO_2 and CH_4, and elevated base metal concentrations [*Shitashima et al.*, 1997; *Douville*, 1999; *Ishibashi et al.*, 1996; *Bach et al.*, 2003]. Analyses of dredged chimney materials gave elevated trace metals including Cu, Zn, Pb, Ba, Au, and Ag [*Scott and Binns*, 1995; *Parr et al.*, 1996; *Moss and Scott*, 2001]. All these characteristics combined to identify PACMANUS as a target for ODP investigations into the nature of back arc, metallogenic hydrothermal activity.

3. Methods

[7] Samples for this study were obtained by rotary coring of altered dacite/rhyodacite during ODP Leg 193 [*Binns et al.*, 2002]. Core recovery overall was typically ~10% (13.9% for Snowcap and 7.4% for Roman Ruins). Specimen depths are given as the depth to the top of the 10 m core that contained each specimen. Because of the recovery limitations, it is not known whether a given sample is from the top, middle, or bottom of the section, so depths are approximate.

[8] Samples of altered volcanic rock with anhydrite veins were vacuum-impregnated with epoxy, cut into thin wafers, and polished on both sides. Wafers were studied petrographically and portions were broken out for microthermometric measurements on a modified U.S. Geological Survey (USGS)-type gas flow stage manufactured by Fluid, Inc. The thermocouple used for measuring the temperature of phase changes in the natural fluid inclusions was calibrated using synthetic fluid inclusion standards having nominal phase changes at −56.6°, 0.0°, and +374°C. Calibration runs indicate that the uncertainties of reported measurements are <0.5°C at −56.6°C, <0.1°C at 0.0°C, and <0.5° at 374°C.

[9] Microthermometric measurements on inclusions hosted by anhydrite involved a number of unconventional challenges. The friable and sometimes vuggy nature of the specimens required vacuum impregnation, and the epoxy progressively discolored, melted, and eventually burned at experimental temperatures exceeding 150–200°C. Many inclusions originally visible became occulted. In addition, homogenization temperatures (Th) had to be measured sequentially as sample temperature was increased, because independent tests showed that overheating by several tens of degrees was sufficient to generate internal overpressures capable of making some inclusions begin to stretch irreversibly (D. A. Vanko and W. Bach, Heating and freezing experiments on aqueous fluid inclusions in anhydrite: recognition and effects of stretching and the low-temperature formation of gypsum, submitted to *Chemical Geology*, 2004, hereinafter referred to as Vanko and Bach, submitted manuscript, 2004). For both these reasons, freezing experiments were always carried out prior to heating experiments.

[10] More specific to the anhydrite host, however, was the problem of fluid-host reaction during the freezing experiments. Upon cooling, most aqueous inclusions in anhydrite ($CaSO_4$) reacted to form variable amounts of gypsum ($CaSO_4 \cdot 2H_2O$). This reaction has been noted before [e.g., *Roedder*, 1984, p. 295], and the potential consequences for inclusion studies have been carefully considered [*Tivey et al.*, 1998]. Experiments to test the identification of the low-temperature phase as gypsum, and to measure the errors involved if gypsum growth is ignored, were conducted (Vanko and Bach, submitted manuscript, 2004). Briefly, it was determined that when gypsum growth became extreme, the ice melting temperatures [Tm(ice)] dropped as the residual liquid in the inclusions became more saline. To assure accurate Tm(ice) measurements, gypsum was eliminated from inclusions when necessary by heating the specimen to 120–130°C, which was sufficient to dehydrate all the gypsum and restore the inclusions to their original salinity.

[11] Overall, 15 samples were investigated by microthermometry. Temperatures of more than 800 individual phase changes were recorded from 530 different fluid inclusions. Paired Tm(ice) and Th determinations were collected from over 265 inclusions. In most cases, for each small group of inclusions for which data were collected, there were many other inclusions, part of the same fluid inclusion assemblage (FIA), which behaved the same way. All of the microthermometric analyses reported here were made in the first author's labs either in Atlanta, Georgia, or Towson, Maryland.

[12] Homogenization temperatures of inclusions for which salinity was determined were corrected for pressure effects assuming the binary NaCl-H_2O system and a hydrostatic pressure gradient of 100 bars/1000 m, using the computer programs of *Bakker* [2003], which incorporate the experimental data of *Bodnar* [1993] and *Zhang and Franz* [1987]. Temperature corrections ranged from 0 to 12°C. The pressure-corrected values are estimates for true trapping temperatures (Tt).

[13] Six specimens were studied using a fluid inclusion crushing stage [*Roedder*, 1984]. The specimens were representative of shallow, intermediate, and deep cores from both drilling sites. The behavior of 24 inclusions was recorded during mechanical crushing in immersion oil.

[14] Other ancillary techniques used to answer specific questions included PIXE-PIGE (proton-induced X-ray

emission and proton-induced gamma ray emission [e.g., *Ryan et al.*, 1995; *Ménez et al.*, 1999; *Vanko et al.*, 2001]), laser Raman microspectroscopy (LRM) and cathodoluminescence (CL). Reconnaissance PIXE-PIGE analyses took place at the CSIRO nuclear microprobe facility, North Ryde, New South Wales, Australia, with the assistance of C. Ryan. Reconnaissance LRM work took place in the Fluids Research Lab at Virginia Tech with the help of R. Bodnar, and at the USGS laboratory in Reston, Virginia, with the help of R. Burruss and I.-M. Chou.

4. Results

4.1. Site 1188, Snowcap

[15] Several ODP drill holes were established at the summit of this knoll (at ~1645 m below sea level), which is characterized by gentle effusion of low-temperature fluids and a coating of white flocculent material (the "snowcap" on the knoll). The two cored holes, Hole 1188A and 1188F, were offset by 30 m, and taken together they provide a vertical section to 387 mbsf [*Binns et al.*, 2002]. Recovery averaged 13.9%, and shipboard studies provided an understanding of the basic lithostratigraphy. Volcanic rocks at the seafloor and extending down to around 35 mbsf are fresh rhyodacite [*Binns et al.*, 2002; *Paulick et al.*, 2004; D. J. Miller et al., Recent magmatic activity at Pual Ridge, Papua New Guinea: Implications for sulfide mineralization in an active, felsic-hosted seafloor hydrothermal system, submitted to *Proceedings of the Ocean Drilling Project, Scientific Results*, vol. 193, 2004]. All of the underlying volcanic rocks are pervasively altered, some to completion. Alteration is highly variable, displaying complex overprinting of acid sulfate (quartz/cristobalite-pyrophyllite-illite-anhydrite) and argillic (quartz/cristobalite-chlorite-smectite) alteration, and local zones of magnetite enrichment [*Binns et al.*, 2002; C. Yeats et al., manuscript in preparation, 2003]. Alteration in many units was controlled by a closely spaced network of fractures that resulted in a variety of pseudoclastic textures. Late stage fractures cutting across textures from the earliest alteration stages are filled by anhydrite with accessory pyrite (Figure 2).

[16] The hydrothermal effluent at Snowcap measured by submersible was only ~6°C, and nearby columnar chimneys on the flank of the knoll are venting 65°C fluid [*Binns et al.*, 1996]. However, the temperature measured at a depth of 360 mbsf in Hole 1188F after only eight days of postdrilling thermal rebound was 313°C.

4.1.1. Anhydrite Veins

[17] Anhydrite-filled fractures (Figure 2) are most abundant in the top 100 m of seafloor beneath Snowcap, but they persist all the way to the deepest units. Specimens with vein anhydrite (with ubiquitous accessory pyrite) were taken from 10 cores, at depths varying from 48 to 354 mbsf. The anhydrite veins vary from about a millimeter to several centimeters in width. Some anhydrite veins have vugs, and most have alteration haloes in the wall rock that are enriched in silica, pyrophyllite, illite and pyrite.

[18] Many anhydrite crystals, particularly large ones centrally located in veins, have one or more cloudy (brownish in thin section and bluish in stereoscopic view) growth zones. These typically outline the simple orthorhombic forms (prism and pinacoid). Intricate zoning at a much finer scale is visible in many cathodoluminescence images.

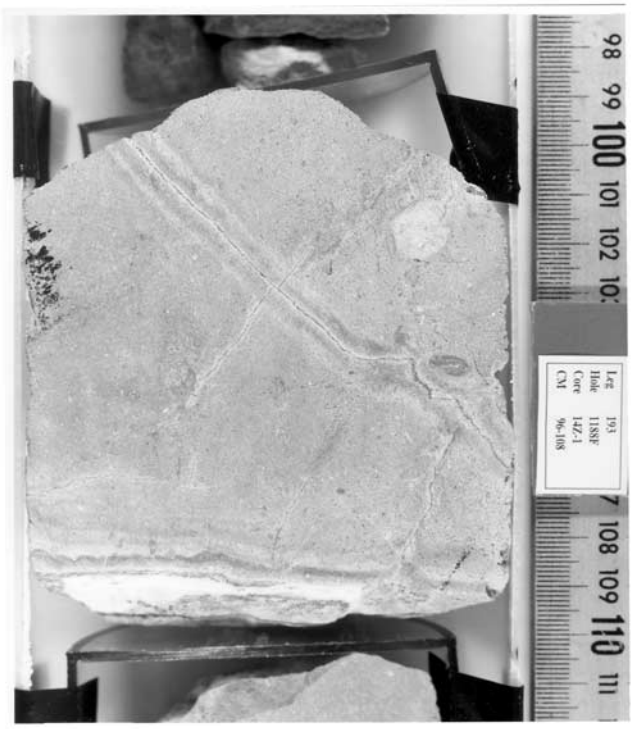

Figure 2. Photograph of a core specimen with typical white anhydrite veins. The sample is from Snowcap at a depth of 246 m below the seafloor.

4.1.2. Fluid Inclusions

[19] Aqueous fluid inclusions ranging from 1–2 μm up to several hundred micrometers in size occur in all the anhydrite veins studied. Their distribution and abundance varies widely, with some crystals being virtually inclusion-free, while others contain abundant inclusions (Figure 3). Inclusion shapes are typically either (1) elongate to acicular rectangular prisms oriented parallel to host crystal axes (Figures 3a and 3b); (2) blocky to rounded rectangular (Figure 3c); or (3) flattened rectangular (Figures 3d and 3e). Rounded irregular shapes also occur, particularly when the inclusions are vapor-rich (Figure 3f). Few inclusions are oriented along crosscutting healed fractures. Instead, most form nonplanar clusters that have similar phase ratios, i.e., they occur in "fluid inclusion assemblages," or FIAs, and are interpreted as primary fluid inclusions that have trapped fluid at the time of original crystal growth (Figure 3b is a good example). Indeed, some elongate inclusions appear to have nucleated in the lee of pyrite grains that are embedded in the host anhydrite, strongly suggesting a primary origin. Despite the occurrence of recognized growth zones in some anhydrite crystals, there appears to be no zoning of fluid inclusion types either with respect to growth zones, or with respect to position within a vein (i.e., close to the wall, in the center).

[20] Three types of inclusions were recognized. Type I inclusions are liquid plus vapor (L+V) that homogenize to liquid (Figures 3a, 3b, and 3c). A small proportion of type I inclusions also contains either an opaque solid phase, commonly fairly large, and/or a tiny transparent solid phase.

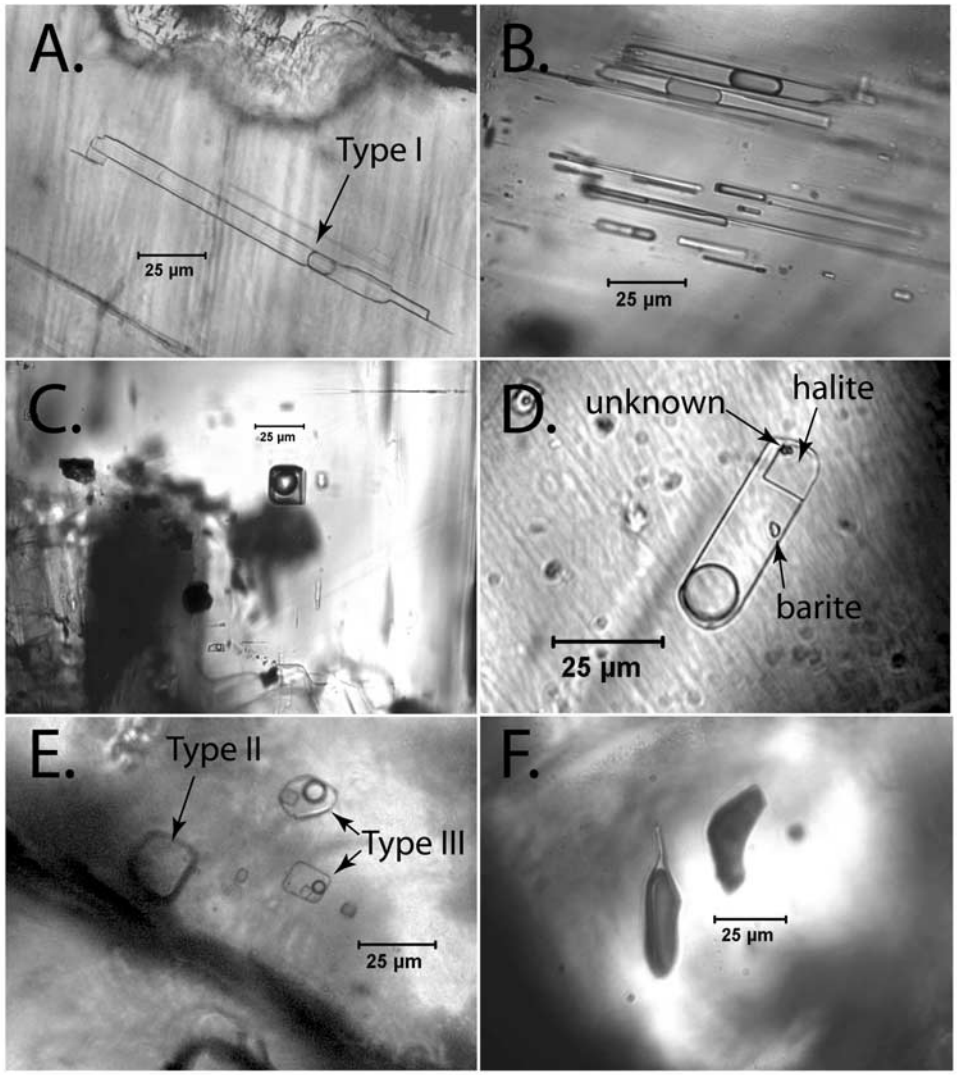

Figure 3. Photomicrographs of representative fluid inclusions in anhydrite veins. Scale bars are 25 μm long. (a) Elongate type I, L+V inclusion, Snowcap, 48 m below the seafloor (mbsf). (b) Group of elongate and acicular type I, L+V inclusions, Roman Ruins, 157 mbsf. These are interpreted as a cogenetic primary fluid inclusion assemblage (FIA). Ice melting temperatures vary from −2.0 to −2.5°C. Homogenization temperatures for three of the inclusions varied from 247 to 265°C. (c) Blocky rectangular type I, L+V inclusion, Snowcap, 300 mbsf. (d) Type III brine-filled inclusion that contains L, V, a cubic halite crystal, a small transparent barite crystal, and a third, unidentified Fe-bearing solid; Snowcap, 126 mbsf. (e) A pair of type III inclusions and a nearby type II inclusion; Snowcap, 126 mbsf. (f) Vapor-rich type II inclusions, which homogenize to vapor; Snowcap, 300 mbsf.

Type II inclusions are L+V that homogenize to vapor (Figures 3e and 3f); this type also includes apparent vapor-only inclusions that almost surely contain a meniscus of water that is unseen. Type III inclusions are brine filled and contain a halite daughter crystal (Figures 3d and 3e). They commonly also contain a tiny transparent solid phase and a tiny opaque solid. The identification of the daughter crystal as halite is based upon (1) cubic form, (2) isotropy (often difficult to determine in the highly birefringent anhydrite host), (3) behavior on freezing (partial or complete hydration to probable hydrohalite) and heating (reproducible dissolution at elevated temperature, followed by renucleation on quenching), and (4) detection of Na by PIGE.

[21] Reconnaissance PIXE studies were carried out on several fairly large, multiphase type III inclusions from a depth of 126 mbsf. Results indicated the presence of significant Fe (about 1000–40,000 ppm Fe), as well as Zn (30–100 ppm), Mg (a few hundred parts per million) and Ba (~20–150 ppm), but Cu was not observed at the detection limit of 20–30 ppm. Characteristic Fe X-ray emission was concentrated at the location of a tiny opaque daughter crystal, while characteristic Ba X-ray emission was concentrated over a tiny transparent daughter crystal.

[22] Samples from 97, 126, and 287 m below the seafloor were studied using a crushing stage. Of the 25 inclusions that were studied carefully, 3 had vapor bubbles that contracted when the inclusions broke, while

Table 1. Summary of Fluid Inclusion Data for Site 1188, Snowcap[a]

Sample	Depth, mbsf	Hydrostatic Pressure, bars	Inclusion Type	Tm(ice) Range	Tm(ice) Mode	Th Range	Th Mode	Tt Range	Tm (halite)	Remarks
193-1188A-7R-1, Pc 12, 66–68 cm	48	169	I	−2.4 to −0.9	−1.5	127–332	160	149–320		
193-1188A-12R-1, Pc 7, 72–74 cm	97	174	I	−2.1 to −0.5	−1.8	112–178	150	120–187		
193-1188A-15R-1, Pc 4, 14–20 cm	126	177	I	−14.5 to −0.1	−1.8	134–385	280	219–385		
			III	−39.9 to −29.5	−35	158–327			125–257	
193-1188A-16R-2, Pc 15, 109–111 cm	135	178	I	−2.2 to −0.2	−1.6	134–330	240	235–324		
193-1188A-17R-2, Pc 2, 6–9 cm	145	179	I	−4.9 to −1.2	−2.3	208–352	290	218–354		
193-1188F-1Z-4, Pc 2, 100–104 cm	218	186	I	−26.4 to −0.1	−1.6	235–336	300	270–375		
			II	−0.2		330–380				Four type II inclusions.
			III			235			228	Single type III inclusion.
193-1188F-7Z-1, Pc 1c, 30–36 cm	235	188	I	−7.6 to −0.1	−0.4	240–359	300	291–360		
			II	−1.6 to −0.1	−0.6	350–374				
193-1188F-23Z-2, Pc 1, 7–9 cm	287	193	I	−3.9 to −0.5	−2.1	301–361	333	311–363		
193-1188F-26Z-1, Pc 4, 62–69 cm	300	194	I	−3.3 to −0.2	−1.5	316–368	360	325–368		
			II	−1.0 to −0.6		350				
193-1188F-39Z-1, Pc 1, 9–12 cm	353	199	I	−33.6 to −0.5	−1.1	303–401	365	331–401		
			II	−1.1						Single inclusion.
			III	−49.1		331, 332			138, 179	Two inclusions.

[a]Temperatures are in degrees Celsius.

12 behaved quite differently. In all 12, as the inclusion was intersected by a fracture, the vapor gently to quickly expanded (depending on how big the fracture was), usually to fill the whole fluid inclusion. This was typically about a 5–10X volume expansion of vapor, as many of the inclusions originally had about 10–20% vapor, and it suggests the initial partial pressure of the gas was around 5–10 atm. After about a minute, the vapor typically contracted and eventually disappeared as it dissolved into the index oil used for crushing.

[23] The crushing results suggest that a small amount of gas such as CO_2 or CH_4 is present in most if not all of the fluid inclusions. If a typical vapor bubble accounts for 10 vol.% of an inclusion and it expands on crushing to fill the inclusion, then the original gas pressure is about 10 atm. Assuming the gas is ideal and the aqueous fluid is water, the mole fraction of gas is then calculated to be 0.08 mol %, or ~5 mM. This value compares very well with the end-member gas concentrations reported by *Ishibashi et al.* [1996] for PACMANUS vents: about 20–40 mM CO_2 and 20–40 μM CH_4.

[24] Several inclusions were investigated by LRM (laser Raman microspectroscopy) to try to identify any Raman-active gases (e.g., CO_2, CH_4), and to identify daughter crystals. Only a small number of samples were investigated, but none of the spectra from vapor bubbles, even in vapor-rich inclusions, contained gas peaks. It is assumed that the gas concentrations, estimated from crushing to be of the order of 0.1 mol %, were below the detection limit of the Raman microprobe technique.

[25] Opaque solids in several inclusions gave Raman spectra consistent with hematite in one case and goethite in another. Neither spectrum is consistent with pyrite, even though pyrite is an accessory phase in the anhydrite veins. It is possible that pyrite was stable originally, but that hydrogen loss by diffusion resulted in the replacement of pyrite by iron oxide [e.g., *Mavrogenes and Bodnar*, 1994]. One tiny transparent solid in an inclusion yielded a Raman spectrum identical to that of barite.

4.1.3. Microthermometric Data

[26] Ice melting temperatures for inclusions at Snowcap (Table 1), vary widely from a high of −0.1°C (i.e., nearly pure water, or just 0.2 wt % NaCl equivalent) to a low of −49.1°C (or very saline, with a eutectic temperature far below that of the NaCl-H_2O binary). A frequency histogram of all the Tm(ice) values (Figure 4) shows a strong mode at about −1.9°C, the ice melting temperature of seawater.

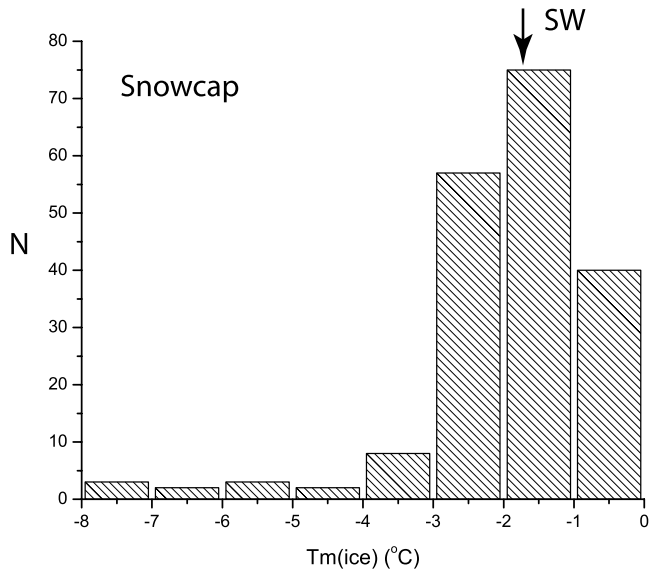

Figure 4. Frequency histogram of Tm(ice) values for Snowcap (Site 1188). Not included are three temperatures between −20.8° to −26.4°C and one at −49.1°C. The arrow indicates the bin where seawater (SW) would fall with a Tm(ice) of about −1.9°C.

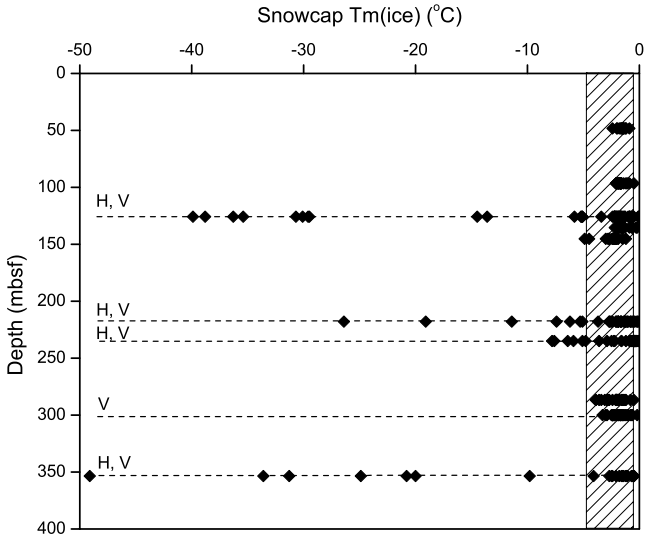

Figure 5. Tm(ice) versus depth in meters below seafloor (mbsf) for Snowcap (Site 1188). V indicates specimens with some inclusions that homogenize to vapor. H indicates specimens with some halite daughter crystals. Both of these features are taken to indicate locations where fluids underwent phase separation (boiling, see text). The patterned strip shows the salinity range observed from active vent fluids worldwide, which is 0.19 to 7.28 wt % NaCl equivalent [from *Von Damm*, 1995] and corresponds to Tm(ice) of −0.1 to −4.6°C. Note that seawater has a Tm(ice) value of −1.9°C. Compared to seawater, inclusions with significantly less saline and more saline compositions are abundant.

Numerous inclusions, though, are much less saline than seawater, and numerous ones are much more saline.

[27] Halite dissolution temperatures for 10 inclusions varied from 125–273°C, implying bulk salinities of 31 ± 3 wt % NaCl equivalent, using the binary NaCl-H_2O as a model system to interpret the microthermometric data (Table 1).

[28] Tm(ice) values plotted as a function of depth (Figure 5) show that there is no relationship between depth and salinity for inclusions at Snowcap. Some specimens contain a relatively restricted set of inclusion salinities, while others contain widely variable salinities.

[29] Homogenization temperatures plotted as a function of depth (Figure 6) exhibit a definite trend, with deep samples containing uniformly higher-temperature inclusions with a narrow temperature range, while shallower samples contain progressively lower-temperature inclusions with a wide temperature range. Thus there are high-temperature inclusions that persist within even the shallowest samples.

[30] Figure 6 also shows the two-phase (boiling) curve for seawater. With rare exceptions, the upper limit of trapping temperature coincides with this boiling curve, suggesting that upwelling fluids at Snowcap frequently intersected the boiling conditions. This is consistent with the widespread distribution of independent inclusion evidence for boiling (type II and type III inclusions) shown in Figure 5.

4.2. Site 1189, Roman Ruins

[31] Two cored drill holes were established in this high-temperature vent field, at a water depth of ~1690 m [*Binns et al.*, 2002]. Hole 1189B is sited directly adjacent to active high-temperature sulfide chimneys and Hole 1189A is located ~30 m away. Beneath a thin crust of fresh rhyodacite, the rocks in Hole 1189A are broadly similar to those from Snowcap. In particular, late stage anhydrite veins are common. This hole went to about 120 mbsf with an average recovery of 6.8% [*Binns et al.*, 2002; *Paulick et al.*, 2004]. The lithostratigraphy of Hole 1189B (7.8% recovery) differs dramatically and includes a soft 70 m pyrite-rich upper zone and a lower 140 m zone that consists of volcanic rocks that are typically less altered than in other holes [*Binns et al.*, 2002; *Paulick et al.*, 2004; C. J. Yeats et al., manuscript in preparation, 2003].

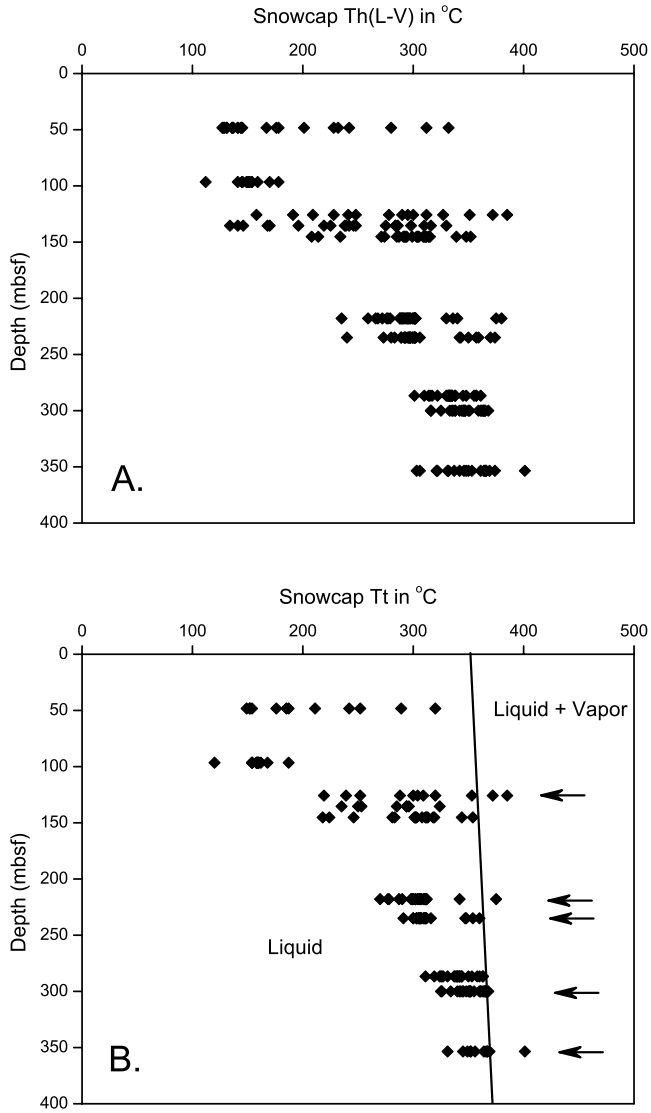

Figure 6. (a) Homogenization temperature versus depth for Snowcap (Site 1188). (b) Trapping temperature versus depth. The trapping temperatures were determined using *Bakker*'s [2003] computer programs. The two-phase (boiling) curve for 3.5 wt % NaCl-H_2O solution (i.e., with seawater salinity) is plotted from the data of *Bischoff and Pitzer* [1989]. Large arrows indicate the sample depths where fluid inclusions provide evidence for phase separation (see Figure 5).

Table 2. Summary of Fluid Inclusion Data for Site 1189, Roman Ruins[a]

Sample	Depth, mbsf	Hydrostatic Pressure, bars	Inclusion Type	Tm(ice) Range	Tm(ice) Mode	Th Range	Th Mode	Tt Range	Tm (halite)	Remarks
193-1189A-3R-1, Pc 11, 65–68 cm	19	171	I	−2.7 to −1.1	−2.5	245–344	310	255–347		
193-1189A-7R-1, Pc 3, 19–23 cm	58	175	I	−3.0 to −1.7	−2.8	312–368	340	320–368		
193-1189B-10R-1, Pc 5, 42–44 cm	118	181	I	−0.1 to −3.6	−2.4	232–349	280	242–352		
			II	−0.3 to −5.2	−2.0					
			III				280		273	one inclusion
193-1189B-14R-1, Pc 17, 123–129 cm	157	185	I	−0.9 to −2.5	−2.3	247–330	250	264–335		
193-1189B-14R-2, Pc 1, 0–3 cm	158	185	I	−3.2 to −1.7	−2.4	318–353	345	326–354		
			II	0.0						two inclusions

[a]Temperatures are in degrees Celsius.

4.2.1. Anhydrite Veins

[32] Specimens from Roman Ruins with vein anhydrite are less abundant, and the veins are thinner, compared to Snowcap. Anhydrite is most common in the upper 50–80 m, with sporadic anhydrite veins down to 160 mbsf [*Binns et al.*, 2002]. Five specimens used for fluid inclusion studies are from cores at depths of 19, 58, 118, 157, and 158 mbsf.

4.2.2. Fluid Inclusions and Microthermometric Data

[33] Aqueous fluid inclusions observed in Roman Ruins samples appear to be very similar to those from Snowcap. Shapes, sizes, and distributions are virtually the same, to the extent that samples from the two sites are petrographically indistinguishable. Crushing experiments carried out on inclusions from specimens at depths of 19, 58, and 158 mbsf yielded results essentially identical to those described previously for Snowcap inclusions. However, microthermometric data for Roman Ruins (Table 2) and Snowcap show distinct differences.

[34] Ice melting temperatures for inclusions at Roman Ruins define a fairly restricted salinity range centered on seawater salinity (Figure 7). Only a few type II inclusions, which homogenize to vapor, were recognized in the samples from 118 and 158 mbsf, and many of these have very low salinities (Tm(ice) = 0°C, indistinguishable from fresh water). A high salinity brine like those that are widespread (if not abundant) beneath Snowcap has been encountered in only one fluid inclusion in the upper 160 m of the subseafloor at Roman Ruins (Table 2).

[35] Homogenization temperatures for inclusions from Roman Ruins are more uniformly high (Figure 8), consistent with the focused fluid flow and high temperature venting now occurring there. As with the case at Snowcap, the upper limit of trapping temperatures coincides with the boiling curve for seawater, indicating that hot, upwelling hydrothermal fluid intersected the boiling curve and generated vapor-rich fluids now trapped in type II inclusions. Much lower temperature fluids have yet to be recognized at Roman Ruins, perhaps indicating that massive cooling and mixing with cold seawater in this upwelling site is less prevalent.

5. Discussion

5.1. Fluid Temperature Regimes

[36] The fluid inclusion temperature profile for Roman Ruins, the focused high-temperature venting site, shows a restricted range of uniformly high-temperature fluids (242–368°C) at all four depths (Figure 8). Similar temperatures have been determined independently from mineral oxygen isotopic compositions: chlorite±illite formed from about 220–250°C, with a quartz overprint at about 350°C [*Lackschewitz et al.*, 2004]. These temperatures reflect the style of present-day fluid flow, which is rapid focused upflow. Many temperatures, though, exceed significantly the maximum vent temperature of 276°C measured by submersible at Roman Ruins, suggesting either that the hottest vent fluids have yet to be sampled, or that vent temperatures in the not-too-distant past were higher than today.

[37] The profile for Snowcap (Figure 6) shows a restricted range of trapping temperatures in the range 270–375°C at depths below 200 mbsf (one sole inclusion "trapped" at 401°C is not really good evidence that fluids reached such a high temperature). However, there is a broadening of the range to temperatures as low as 152°C toward the seafloor (again, with one sole inclusion having an unusually low "trapping temperature" of 120°C). Temperatures calculated by *Lackschewitz et al.* [2004] from clay minerals at Snowcap yield similar values, from about 220°C (chlorite ± illite)

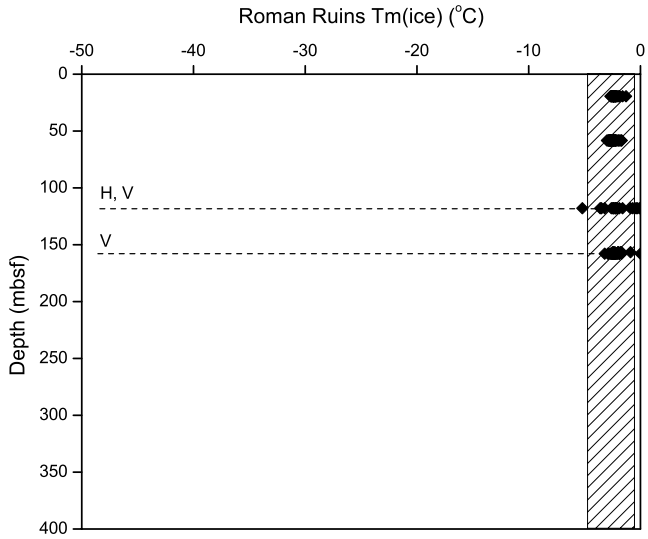

Figure 7. Tm(ice) versus depth for Roman Ruins (Site 1189). V indicates specimens with some inclusions that homogenize to vapor. H indicates one specimen where a halite daughter crystal was observed. The patterned strip represents the salinity range observed from active vent fluids worldwide. Note that seawater has a Tm(ice) value of −1.9°C. Compared to Snowcap (Figure 5, which is plotted at the same scale), salinity variations at Roman Ruins are more restricted.

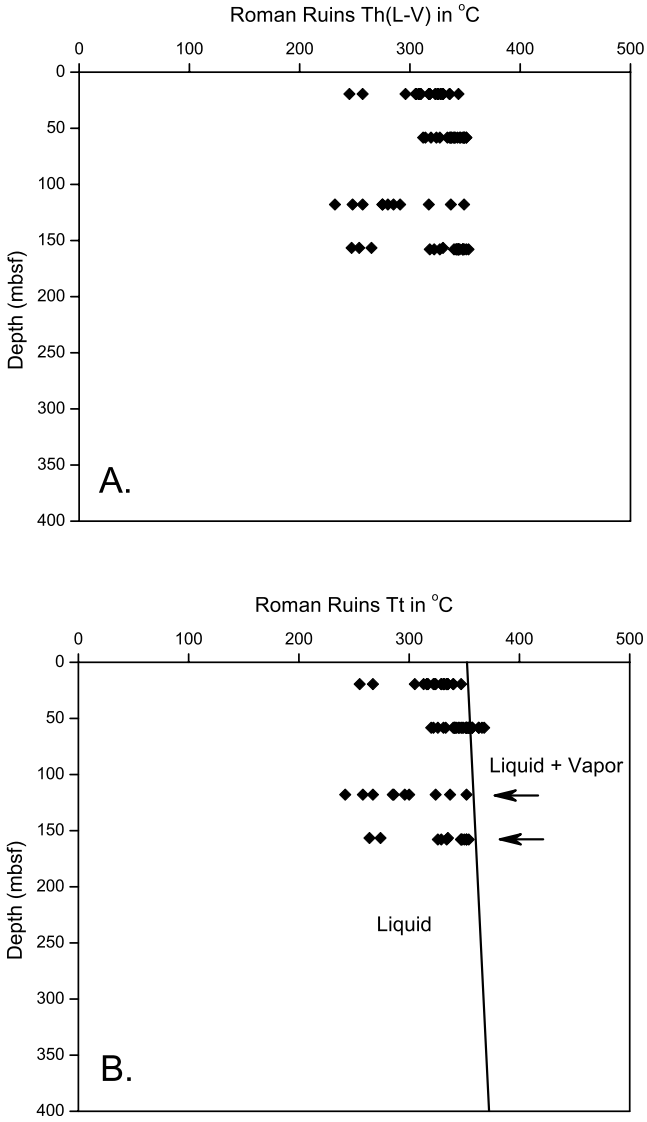

Figure 8. (a) Homogenization temperature versus depth for Roman Ruins (Site 1189). (b) Trapping temperature versus depth. The trapping temperature determination and the location of the seawater boiling curve are explained in the caption of Figure 6b. Large arrows indicate the sample depths where fluid inclusions provide evidence for phase separation (see Figure 7).

to as high as 315°C (pyrophyllite). A curve connecting the lowest trapping temperatures as a function of depth suggests a concave-downward advective thermal gradient that may reflect today's gentle fluid flow regime at Snowcap. This is consistent with the ODP borehole measurement of 313°C at 360 mbsf, while present-day active effluent at the seafloor occurs at temperatures of just a few degrees to tens of degrees Celsius. Fluids cooler than 150°C are undoubtedly present at depths shallower than 100 mbsf, but these generally cannot be trapped in anhydrite, which forms at $T \geq 150$°C.

[38] Despite evidence that the present-day temperature in the shallow subseafloor at Snowcap is rather low, the fluid inclusion record from shallow samples contains evidence for the past presence of a range of both moderate-temperature (e.g., ≥150°C) and quite high-temperature (e.g., approaching 375°C) fluids. This suggests that previously, rather high-temperature fluids were close to the seafloor and were probably venting at focused chimney sites, now gone. In other words, the subseafloor thermal profile at Snowcap in the past may have resembled what is seen at Roman Ruins today. The fluid inclusion record is not clear enough to determine whether there may have been a single high-temperature event followed by waning conditions, or whether there might have been multiple events. However, the complex overprinting relationships present in altered rocks from the upper 150 m of the sequence at Snowcap tend to support the latter hypothesis [*Binns et al.*, 2002; C. J. Yeats et al., manuscript in preparation, 2003].

[39] An additional process inferred from the Snowcap Tt profile is that hot fluids rising from depth are cooled to varying degrees by mixing and entrainment of cold seawater-salinity groundwater. This contrasts with the situation at Roman Ruins, where hot hydrothermal fluids ascend rapidly and vent through chimneys at the seafloor [*Binns et al.*, 1996]. At Roman Ruins, the high-T ascent paths may be isolated from seawater-like groundwater by an impermeable cylinder of fractured rock cemented with anhydrite [*Lowell and Yao*, 2002]. The rocks cored at Snowcap may resemble such an anhydrite-cemented column, showing fluid inclusion evidence for the passage of high-temperature hydrothermal fluid as well as various proportions, increasing with decreasing depth, of mixing with ambient groundwater.

[40] Cathodoluminescence images showing variable luminescence colors and complex zoning patterns appear to reveal evidence that fluid parameters varied significantly. Although the direct cause and effect for the cathodoluminescence features is not understood, the images support the interpretation that a given fracture, while being filled by precipitating anhydrite, must have seen the passage of fluids of varying temperature and composition, completely consistent with the microthermometric data.

5.2. Fluid Compositions and Origin

[41] Modern black smoker fluids are known to vary significantly from seawater salinity primarily as a result of phase separation processes [e.g., *Von Damm et al.*, 1997, 2003]. Most of the fluids from the subseafloor at Roman Ruins exhibit salinity variations that fall within the range observed at modern active mid-ocean ridge hydrothermal fields (0.2–7.3 wt % NaCl [*Von Damm*, 1995]). However, one specimen from Roman Ruins contains a small number of inclusions that contain essentially pure water. These are vapor-rich inclusions that homogenize to vapor and exhibit ice melting at 0°C. This fluid is less saline than any fluid yet sampled from modern active vents, and must essentially represent distilled water formed by boiling. However, such a low-salinity fluid is by no means unexpected given the physical setting: when NaCl-H_2O solutions with the salinity of seawater boil at temperatures between 350 and 400°C and pressures between 160 and 200 bars, the vapor phase has salinities below 0.05 wt % NaCl [*Bischoff and Pitzer*, 1989].

[42] While most of the Roman Ruins fluid inclusions have relatively restricted salinity variations (Figure 7), those from Snowcap exhibit much wider variations (Figure 5).

The majority of inclusions have close-to-seawater salinities, but a significant minority contains either very low salinity or very high salinity fluid. Those with low salinity reach ice melting temperatures as high as −0.1°C, or only 0.18 wt % NaCl equivalent. As at Snowcap, these low-salinity fluids are most likely vapor that boiled off of hydrothermal seawater at temperatures and pressures easily achieved within or just below the drilled sections of Pual Ridge. More saline vapors in inclusions probably represent heterogeneous trapping of a 0.2 wt % vapor and more saline hydrothermal fluid.

[43] While low-salinity inclusions have quite high ice melting temperatures, the saline, type I, L+V inclusions have ice melting temperatures as low as −49°C. With maximum salinities of 31±3 wt % NaCl equivalent, such brines could be formed by closed-system equilibrium phase separation of seawater between about 390°C and 380°C (for P between 200 bars and 165 bars, which is the hydrostatic pressure range within the cored interval at Snowcap) [*Bischoff et al.*, 1986; *Bischoff and Pitzer*, 1989; *Bodnar et al.*, 1985]. Alternatively, vapor may have formed and then segregated from the upwelling hydrothermal fluid at any temperature that exceeded the boiling curve, e.g., at T $\geq$ 350°C (Figures 6 and 8), driving the residual hydrothermal fluid to higher salinities.

[44] Fluid inclusions with very low Tm(ice) values indicate that the fluids are complex multicomponent brines. Cations or elements known to be present include Na^{+}, based upon the seawater source and the occurrence of halite daughter crystals, Ca^{++}, based upon the fact that the host mineral is anhydrite, Fe, based upon the presence of hematite and goethite in some inclusions and of pyrite as an accessory in the veins, Ba^{++}, based upon the presence of barite daughter crystals, and Zn and Mg, based upon PIXE spectra. Other cations possibly present in significant concentrations could include K^{+} and Mn^{++}.

[45] More than 265 paired Th and Tm(ice) measurements were made on fluid inclusions. A plot of Tt versus Tm(ice) (Figure 9) shows that the broad salinity variations indicative of phase separation are restricted to the higher-temperature fluid inclusions, with Th > 300°C or so. This is consistent with brine generation at elevated temperatures followed by conductive cooling, because phase equilibria in the NaCl-H_2O system require temperatures >350°C at the PACMANUS pressures to generate phase separation (Figures 6 and 8).

[46] In addition to the type I brines, some inclusions from Snowcap (and one from Roman Ruins) are halite-bearing type III. These, too, represent brines, and their halite dissolution temperatures suggest an equivalent NaCl concentration of about 31±3 wt %. This simplification, though, neglects the multicomponent nature of the fluids already established. Eight inclusions (from various samples, and therefore not a FIA) have Tm(halite) between 138° and 273°C; thus their equivalent NaCl concentrations range from about 28 to 33 wt % (Figure 10). Their homogenization occurs at higher temperatures, which are plotted in Figure 10 along the liquid-vapor curve for 30 wt % NaCl. These inclusions were trapped at pressures between 177 and 199 bars (assuming a hydrostatic pressure gradient). Therefore, the trapping conditions for these inclusions are defined theoretically by the intersections of the inclusion isochores and the appropriate isobars. Trapping temperatures determined this way vary from about 210 to 350°C, very similar to the less saline type I inclusions. Because the phase separation of seawater salinity fluid at these pressures requires temperatures of about 350–370°C (Figures 6 and 8), some of the type III inclusions must have trapped brine that cooled to varying extents after phase separation and segregation of the brine from its conjugate vapor.

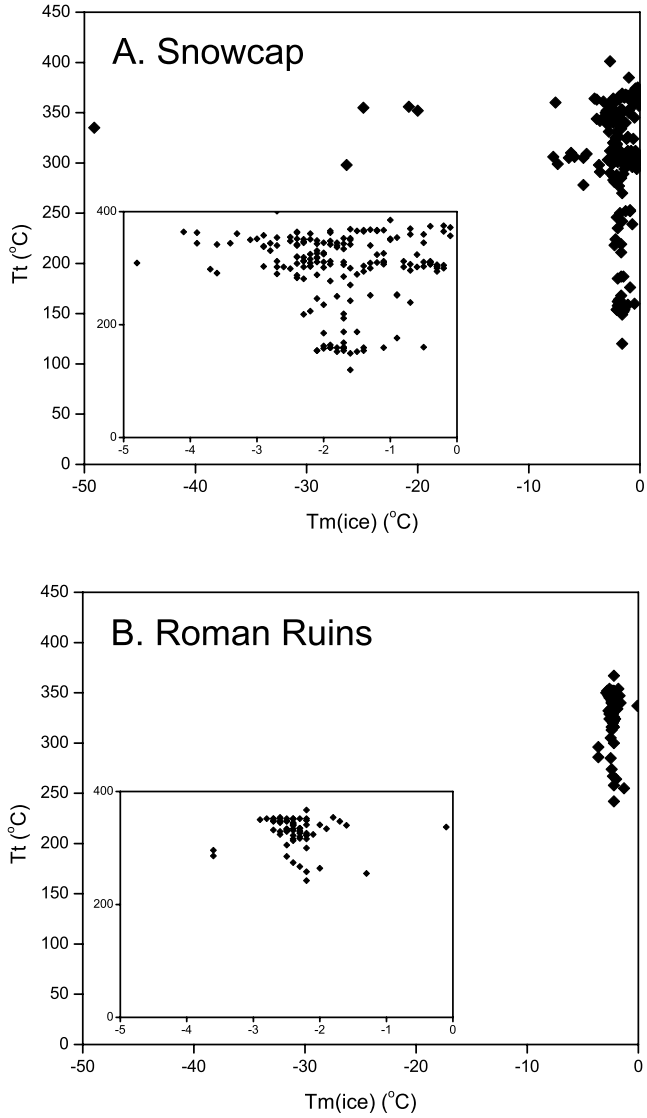

Figure 9. Plots of trapping temperature versus ice melting temperature. (a). Tt versus Tm(ice) for Snowcap (Site 1188). (b) Tt versus Tm(ice) for Roman Ruins (Site 1189). The insets show that portion of the data with Tm(ice) between 0 and −5°C.

[47] One type III fluid inclusion lost its vapor bubble on heating at 158°C, and then homogenized by halite dissolution at 207°C. This is unusual because it implies that the fluid reached halite saturation first on cooling to 207°C (but at a rather high pressure of about 500 bars), prior to reaching the vapor pressure at 158°C. These conditions appear to be unreasonable, and the alternative explanation that this inclusion suffered postentrapment changes is more likely.

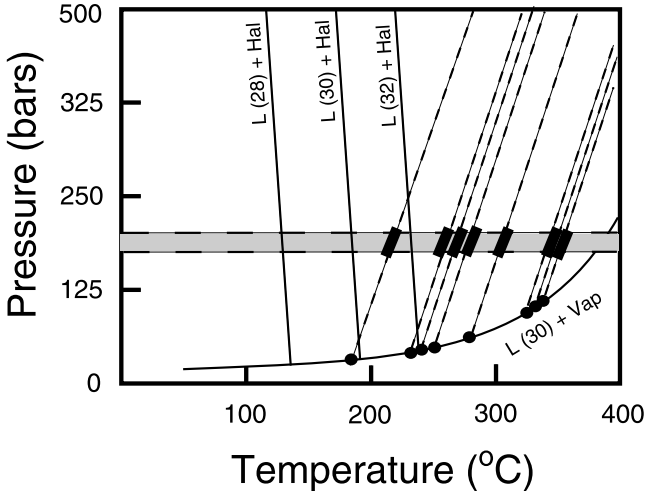

Figure 10. Binary NaCl-H_2O phase diagram for some of the halite-bearing inclusions. The lines with negative slopes represent the approximate halite saturation limits (liquidus curves) for fluids containing 28 through 32 wt % NaCl. The solid curve [L(30)+Vap] is the approximate liquid + vapor curve for a 30 wt % NaCl composition. Solid points along this curve are plotted at the L-V homogenization temperatures of eight type III fluid inclusions from Snowcap. The dashed lines with positive slopes approximate the isochores for these eight inclusions, and the horizontal dashed isobars bracket the hydrostatic pressure range within the Snowcap borehole (shaded horizontal region). Intersections of the isochores and the isobars give the approximate fluid inclusion trapping conditions (black rectangles). The diagram was constructed on the basis of data from *Bischoff and Pitzer* [1989], *Bodnar et al.* [1985], and *Bodnar* [1994].

[48] Brines are present in at least four different anhydrite vein samples beneath Snowcap, at depths of 126, 218, 235, and 354 mbsf. They are not restricted to the deepest portion of the hydrothermal system, as might be expected in a layered system [*Bischoff and Rosenbauer*, 1989]. In a study of seafloor vent chimney samples from another back arc setting, the Lau Basin, *Lécuyer et al.* [1999] described two halite-bearing fluid inclusions with about 30 wt % equivalent NaCl within anhydrite from a chimney sample. *Lécuyer et al.* [1999] suggested that these saline brines might have been erupted through chimneys to the seafloor. It would not be at all surprising if brines are currently being emitted or have been vented through chimneys in the past at Snowcap.

5.3. Correlation With Sr-Isotopic Data

[49] Profiles of strontium isotopic ratios determined from anhydrite grains [*Roberts et al.*, 2003] reveal a significant contrast between Snowcap and Roman Ruins. At Snowcap, the most radiogenic strontium occurs just beneath the unaltered dacite cap that covers the knoll, while deeper anhydrite veins contain much less radiogenic strontium (Figure 11a). *Roberts et al.* [2003] interpret this change to reveal variable mixing between a deep hydrothermal fluid (inferred to have $^{87}Sr/^{86}Sr$ of about 0.705) and cold seawater ($^{87}Sr/^{86}Sr$ = 0.70918). The amount of seawater varies from near zero to about 86% with the highest degrees of seawater entrainment taking place in the shallowest part of the system, just beneath the fresh dacite cap. Trapping temperatures of fluid inclusions (Figure 11b) show that the thermal gradient mirrors the isotopic gradient–deep fluids are uniformly high-temperature and dominated by relatively nonradiogenic hydrothermal fluid, while the shallowest samples show much cooler temperatures caused by mixing with cold seawater and conductive cooling.

[50] In contrast to Snowcap, the strontium isotopic ratios from Roman Ruins show no clear trend with depth, consistent with the fact that trapping temperatures are fairly uniform with depth (Figures 11c and 11d).

[51] Isoenthalpic mixing of cold seawater and a hypothetical 360°C hydrothermal end-member fluid, at the proportions suggested by the Sr-isotopic values, leads to calculated fluid temperatures that can be compared to the trapping temperatures of fluid inclusions from Snowcap (Table 3). For the low-percentage seawater mixes at depths below ~200 mbsf, the Tt and ''mixing temperature'' values closely match (Figure 12). At shallower levels, though, temperatures generally diverge such that the isotopic mixing temperatures progressively exceed the inclusion trapping temperatures (Figure 12). This could be explained if the 360°C end-member fluid cooled somewhat prior to mixing with seawater at the ratio dictated by the Sr-isotope data. In contrast, for the shallowest sample, the inclusion temperatures exceed the isotopic temperature. This could indicate that, here, the cold seawater became heated prior to mixing with the hydrothermal fluid in the required ratio.

[52] Data from anhydrite precipitated within the active TAG hydrothermal mound suggest that seawater entrained into the mound was heated to between 100 and 180°C prior to mixing with upwelling hydrothermal fluid [*Teagle et al.*, 1998]. A similar magnitude of heating of seawater is recorded in the shallowest sample from Snowcap (Figure 12). However, deeper samples from Snowcap, between about 50 and 200 mbsf, document for the first time an additional process (Figure 12). Upwelling hydrothermal fluids must have cooled by up to 100–150°C or so if the assumptions that went into the temperature calculations are valid. Independently, similar amounts of cooling of the hydrothermal fluids are suggested from the trapping temperatures of saline type I fluid inclusions (Figure 9) as well as several type III inclusions, which must have been generated at temperatures greater than 350°C, but were trapped at temperatures as low as about 210°C (Figure 10).

6. Conclusions

[53] 1. High temperature hydrothermal fluids (150 to 385°C) were responsible for precipitating vein anhydrite beneath the PACMANUS hydrothermal field.

[54] 2. At Roman Ruins, a site of active high-temperature venting (220–276°C, measured by submersible), the fluid inclusion thermal profile is uniform and high temperature (242–368°C).

[55] 3. At Snowcap, a site of warm water effusion (6°C to up to 65°C nearby, measured by submersible), the fluid inclusion profile indicates uniform high temperatures at depth (270–385°C), but a wider range of temperatures down to 150°C and probably lower in the shallower section (anhydrite, which forms at T > 150°C, does not trap lower-temperature primary inclusions). This indicates a fluid flow

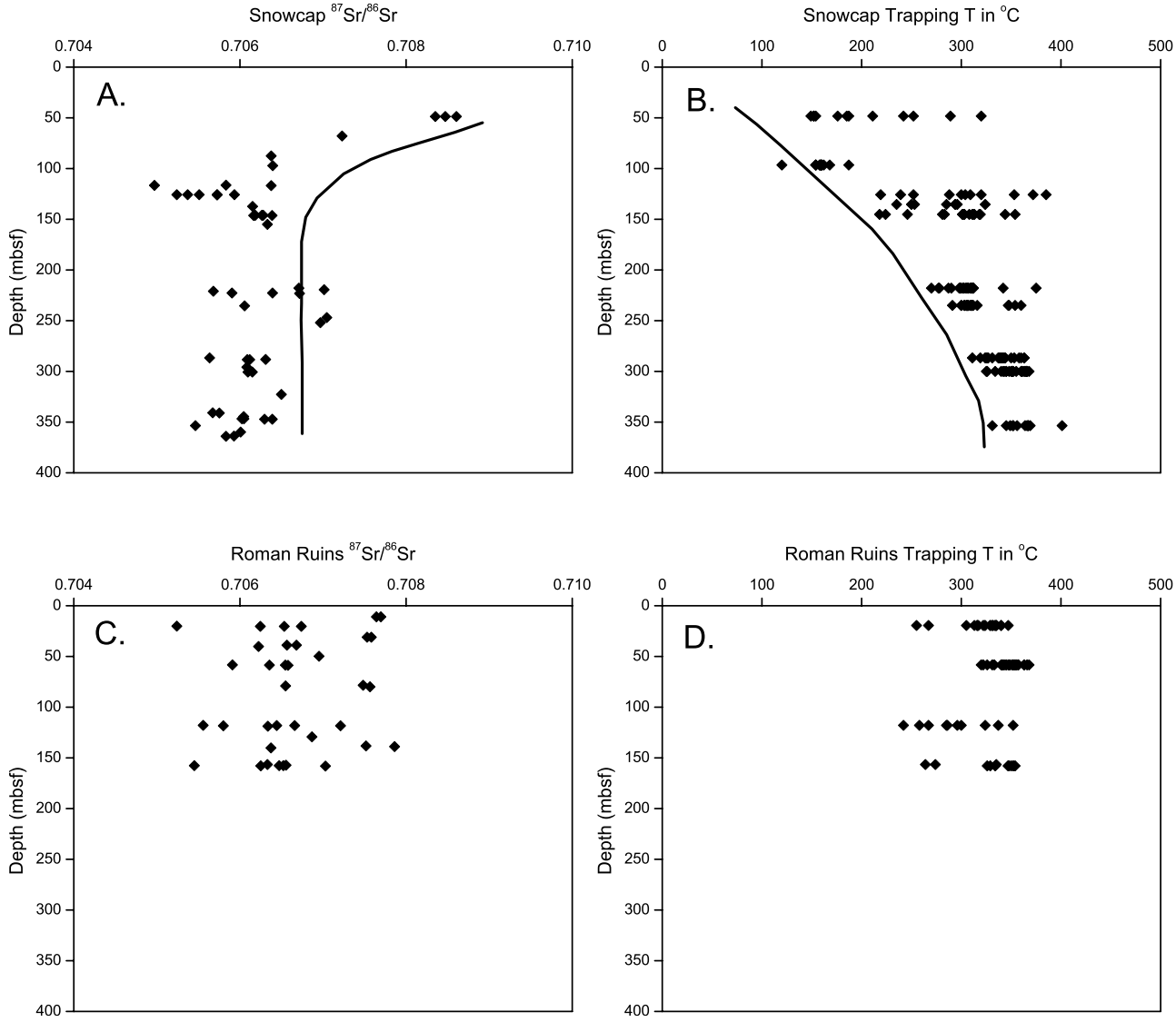

Figure 11. Plots showing the Sr-isotopic ratio of anhydrite veins as a function of depth [*Roberts et al.*, 2003], compared to the trapping temperature of fluid inclusions versus depth (this study). (a) Sr-isotopic ratios for Snowcap (Site 1188). (b) Trapping temperatures for Snowcap. (c) Sr-isotopic ratios for Roman Ruins (Site 1189). (d) Trapping temperatures for Roman Ruins. Note that the Snowcap data form concave-downward arrays, discussed in the text.

Table 3. Sr-isotope and Tt Calculations for Snowcap (Site 1188)[a]

Hole	Core	Section	Interval	Piece	Depth, mbsf	$^{87}Sr/^{86}Sr$ in Anhydrite	F(sw)	Ta, °C	Tb, °C	Tt (avg)	Ta (°C) - Tt (avg)	Tt min	Tt max
1188A	7R	1	66–68	12	48.68	0.708352	0.802	148	75	206	−58	149	320
1188A	12R	1	72–74	7	97.32	0.706394	0.333	335	241	158	177	120	187
1188A	15R	1	14–20	4	125.81	0.705241	0.058	358	339	304	54	219	385
1188A	16R	2	109–111	15	137.95	0.706152	0.276	343	262	279	64	235	324
1188A	17R	2	6–9	2	146.36	0.706387	0.332	335	242	296	39	218	354
1188F	1Z	4	100–104	2	222.65	0.706393	0.333	335	241	305	30	270	375
1188F	7Z	1	30–36	1c	235.3	0.706056	0.253	346	270	313	33	291	360
1188F	23Z	2	30–33	3B	288.4	0.706116	0.267	344	265	340	4	311	363
1188F	23Z	2	34–36	3C	288.44	0.706089	0.261	345	267	340	5	311	363
1188F	26Z	1	62–69	4	300.72	0.706095	0.262	344	267	352	−8	325	368
1188F	39Z	1	0–3	1	353.5	0.705464	0.111	356	320	361	−5	331	401

[a]The $^{87}Sr/^{86}Sr$ values are from *Roberts et al.* [2003]. F(sw) is the fraction of seawater mixed with hydrothermal fluid based on the Sr-isotopes. Ta is isoenthalpic mixing temperature assuming a hydrothermal end-member of 360°C and using the *Bischoff and Rosenbauer* [1985] heat capacity values for 200 bars. Tb is the corresponding "linear" mixing temperature, ignoring energy conservation, and Tt is fluid inclusion trapping temperature.

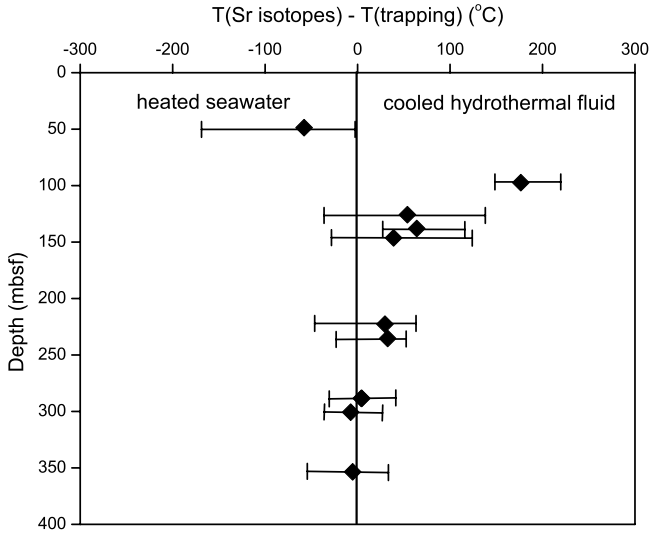

Figure 12. Plot showing the difference, as a function of depth, between the fluid temperature calculated from the isoenthalpic mixing of cold seawater with a hypothetical 360°C hydrothermal end-member fluid (using the proportions dictated by the Sr-isotopic ratio of the anhydrite), and the fluid temperature determined independently from the average (symbol) and range (bars) of inclusion trapping temperatures. Where ΔT is close to zero, the inclusion trapping temperature agrees well with the fluid temperature resulting from isotopically constrained mixing of cold seawater and 360°C hydrothermal fluid. Positive ΔT values suggest that the assumed hydrothermal T of 360°C is too high and therefore suggest that the hydrothermal fluid cooled prior to mixing. Negative ΔT values, on the other hand, suggest that seawater was heated prior to mixing.

regime dominated by vertical advection plus shallow subseafloor entrainment and mixing of cool seawater.

[56] 4. Fluid inclusions at Snowcap exhibit extreme salinity variations indicative of subseafloor boiling. Brine inclusions contain Na, Cl, Fe, Zn, Mg and Ba, and minor amounts (of the order of 0.1 mol %, or 5 mM) of compressed gas such as CO_2 or CH_4. Phase separation occurred at temperatures exceeding about 350°C.

[57] 5. Most fluid inclusions at Roman Ruins exhibit more restricted salinity variations that fall generally within the range of salinities observed at modern active vent sites along the mid-ocean ridge system.

[58] 6. Fluid inclusion temperatures support the hypothesis, developed from Sr-isotopic analysis, that the subseafloor at Snowcap is a site of systematic mixing between deep-sourced hot hydrothermal fluids and cold seawater-like fluid. In contrast, the subseafloor regime at Roman Ruins is less varied, with uniformly high-temperature fluids characterized by hydrothermally dominated Sr-isotopic ratios.

[59] 7. The deepest specimens from Snowcap show that ~360°C hydrothermal fluid mixed isoenthalpically with cold seawater to produce the vein anhydrite. At shallower levels, between 50 and 200 mbsf, the hydrothermal fluid appears to have cooled conductively prior to mixing with cold seawater, and at a very shallow level (50 mbsf), entrained seawater appears to have been heated conductively prior to mixing and anhydrite precipitation.

[60] **Acknowledgments.** We gratefully acknowledge the Ocean Drilling Program and its staff, as well as the Master and crew of the *Joides Resolution* that made Leg 193 a success. Barbara Brocks and Buffy Chournos polished the fluid inclusion samples, and Katie Gatton helped interpret laser Raman microprobe data. Ed Roedder is thanked for an encouraging review of the first draft of the manuscript. We thank Bob Bodnar, Bob Burruss, and I.-Ming Chou for assistance in the laser Raman analyses and Jeff Alt and Bob Bodnar for very helpful reviews on behalf of the journal. Bob Bodnar also donated a custom-made Virginia Tech Department of Geological Sciences fluid inclusion crushing stage for this study. W.B. and D.A.V. thank JOI/USSAC for support and S.R. acknowledges a NERC grant (NER/T/S/2000/0024). This research used samples and/or data provided by the Ocean Drilling Program (ODP). ODP is sponsored by the U.S. National Science Foundation (NSF) and participating countries under the management of Joint Oceanographic Institutions (JOI), Inc.

References

Alt, J. C. (1995), Subseafloor processes in mid-ocean ridge hydrothermal systems, in *Seafloor Hydrothermal Systems, Physical, Chemical, Biological and Geological Interactions*, *Geophys. Monogr. Ser.*, vol. 91, edited by S. E. Humphris et al., pp. 85–114, AGU, Washington, D. C.

Alt, J. C. (1999), Hydrothermal alteration and mineralization of oceanic crust: Mineralogy, geochemistry, and processes, in *Volcanic-Associated Massive Sulfide Deposits: Processes and Examples in Modern and Ancient Settings*, *Rev. Econ. Geol.*, vol. 8, edited by C. T. Barrie and M. D. Hannington, pp. 133–155, Nat. Resour. Can., Miner. Resour. Div., Ottawa, Ont.

Alt, J. C., and D. A. H. Teagle (2000), Hydrothermal alteration and fluid fluxes in ophiolites and oceanic crust, in *Ophiolites and Ocean Crust: New Insights From Field Studies and the Ocean Drilling Program*, edited by Y. Dilek et al., *Spec. Pap. Geol. Soc. Am.*, *349*, 273–282.

Alt, J. C., et al. (1996), Hydrothermal alteration of a section of upper oceanic crust in the eastern equatorial Pacific: A synthesis of results from Site 504B (DSDP legs 69, 70, and 83, and ODP legs 111, 137, 140, and 148), *Proc. Ocean Drill. Program Sci. Results*, *148*, 417–434.

Auzende, J. M., and T. Urabe, and the Shipboard Scientific Party (1996), Submersible observation of tectonic, magmatic and hydrothermal activity in the Manus Basin (Papua New Guinea), *Eos Trans. AGU*, *77*(22), West. Pac. Geophys. Meet. Suppl., W115.

Bach, W., S. R. Roberts, D. A. Vanko, R. A. Binns, C. J. Yeats, P. Craddock, and S. E. Humphris (2003), Controls of fluid chemistry and complexation on rare earth element contents of anhydrite from the PACMANUS subseafloor hydrothermal system, Manus Basin, Papua New Guinea, *Miner. Deposita*, *38*, 916–935, doi:10.1007/s00126-002-0325-0.

Bakker, R. J. (2003), Package FLUIDS 1, Computer programs for analysis of fluid inclusion data and for modelling bulk fluid properties, *Chem. Geol.*, *194*, 3–23.

Binns, R. A., and S. D. Scott (1993), Actively forming polymetallic sulfide deposits associated with felsic volcanic rocks in the eastern Manus back-arc basin, Papua New Guinea, *Econ. Geol.*, *88*, 2226–2236.

Binns, R. A., J. M. Parr, J. C. Waters, J. B. Gemmell, R. Moss, S. D. Scott, J. Naka, J.-L. Charlou, K. Gena, and P. M. Herzig (1996), Actively-forming sulfide deposits at the PACMANUS hydrothermal field, eastern Manus Basin, Papua New Guinea, *Eos Trans. AGU*, *77*(22), West. Pac. Geophys. Meet. Suppl., W115–W116.

Binns, R. A., S. D. Scott, J. B. Gemmell, and K. A. W. C. Crook (1997), The SuSu Knolls hydrothermal field, eastern Manus Basin, Papua New Guinea, *Eos Trans. AGU*, *78*(46), Fall Meet. Suppl., F772.

Binns, R. A., et al. (2002), *Proceedings of the Ocean Drilling Program, Initial Reports* [CD-ROM], vol. 193, Ocean Drill. Program, College Station, Tex.

Bischoff, J. L., and K. S. Pitzer (1989), Liquid-vapor relations for the system NaCl-H_2O: Summary of the P-T-x surface from 300° to 500°C, *Am. J. Sci.*, *289*, 217–248.

Bischoff, J. L., and R. J. Rosenbauer (1985), An empirical equation of state for hydrothermal seawater (3.2 percent NaCl), *Am. J. Sci.*, *285*, 725–763.

Bischoff, J. L., and R. J. Rosenbauer (1989), Salinity variation in submarine hydrothermal systems by layered double-diffusive convection, *J. Geol.*, *97*, 613–623.

Bischoff, J. L., R. J. Rosenbauer, and K. S. Pitzer (1986), The system NaCl-H_2O: Relations of vapor-liquid near the critical temperature of water and of vapor-liquid-halite from 300° to 500°C, *Geochim. Cosmochim. Acta*, *50*, 1437–1444.

Bodnar, R. J. (1993), Revised equation and table for determining the freezing point depression of H_2O-NaCl solution, *Geochim. Cosmochim. Acta*, *57*, 683–684.

Bodnar, R. J. (1994), Synthetic fluid inclusions, XI, The system H_2O-NaCl: Experimental determination of the halite liquidus and isochores for a 40 wt% NaCl solution, *Geochim. Cosmochim. Acta*, *58*, 1053–1063.

Bodnar, R. J., C. W. Burnham, and S. M. Sterner (1985), Synthetic fluid inclusions in natural quartz, III, Determination of phase equilibrium properties in the system H_2O-NaCl to 1000°C and 1500 bars, *Geochim. Cosmochim. Acta*, *49*, 1861–1873.

Davis, E. E., et al. (1992), *Proceedings of the Ocean Drilling Program, Initial Reports*, vol. 139, Ocean Drill. Program, College Station, Tex.

Douville, E. (1999), Les fluids hydrothermaux oceaniques comportement geochimique des elements traces et des terres rares: Processus accocies et modelisation thermodynamique, Ph.D. thesis, Univ. of Brest, Brest, France.

Douville, E., P. Bienvenu, J.-L. Charlou, J.-P. Donval, Y. Fouquet, P. Appriou, and T. Gamo (1999), Yttrium and rare earth elements in fluids from various deep-sea hydrothermal systems, *Geochim. Cosmochim. Acta*, *63*, 627–643.

Fouquet, Y., et al. (1998), *Proceedings of the Ocean Drilling Program, Initial Reports*, vol. 169, Ocean Drill. Program, College Station, Tex.

Gamo, T., K. Okamura, C.-L. Charlou, T. Urabe, J.-M. Auzende, J. Ishibashi, K. Shitashima, and H. Chiba (1997), Acidic and sulfate-rich hydrothermal fluids from the Manus back-arc basin, Papua New Guinea, *Geology*, *25*, 139–142.

Gu, C., and D. A. Vanko (1996), Nature of fluid inclusions in samples of the deep sheeted dikes cored during Leg 148(Hole 504B), *Proc. Ocean Drill. Program Sci. Results*, *148*, 87–95.

Herzig, P. M., S. E. Humphris, D. J. Miller, and R. A. Zierenberg (1998), *Proceedings of the Ocean Drilling Program, Scientific Results*, vol. 158, Ocean Drill. Program, College Station, Tex.

Honnorez, J., J. C. Alt, and S. E. Humphris (1998), Vivisection and autopsy of active and fossil hydrothermal alterations of basalt beneath and within the TAG hydrothermal mound, *Proc. Ocean Drill. Program Sci. Results*, *158*, 231–254.

Humphris, S. E., et al. (1995), The internal structure of an active sea-floor massive sulfide deposit, *Nature*, *377*, 713–716.

Humphris, S. E., et al. (1996), *Proceedings of the Ocean Drilling Program, Initial Reports*, vol. 158, Ocean Drill. Program, College Station, Tex.

Ishibashi, J., et al. (1996), Chemical characteristics of hydrothermal fluids from the Manus back-arc basin, Papua New Guinea, II, Gas components, *Eos Trans. AGU*, *77*(22), West. Pac. Geophys. Meet. Suppl., W116.

Ishibashi, J., T. Yamanaka, K. Okamura, T. Gamo, J-L. Charlou, H. Chiba, K. Shitashima, and H. Takahashi (1997), Geochemical studies of magmatic hydrothermal activity in the DESMOS Cauldron, Manus back arc basin, *JAMSTEC J. Deep Sea Res.*, *13*, 243–248.

Lackschewitz, K. S., C. W. Devey, P. Stoffers, R. Botz, A. Eisenhauer, M. Kummetz, M. Schmidt, and A. Singer (2004), Mineralogical, geochemical and isotopic characteristics of hydrothermal alteration processes in the active, submarine, felsic-hosted PACMANUS field, Manus Basin, Papua New Guinea, *Geochim. Cosmochim. Acta*, in press.

Lécuyer, C., M. Dubois, C. Marignac, G. Gruau, Y. Fouquet, and C. Ramboz (1999), Phase separation and fluid mixing in subseafloor back arc hydrothermal systems: A microthermometric and oxygen isotope study of fluid inclusions in the barite-sulfide chimneys of the Lau Basin, *J. Geophys. Res.*, *104*, 17,911–17,927.

Lowell, R. P., and Y. Yao (2002), Anhydrite precipitation and the extent of hydrothermal recharge zones at ocean ridge crests, *J. Geophys. Res.*, *107*(B9), 2183, doi:10.1029/2001JB001289.

Mavrogenes, J. A., and R. J. Bodnar (1994), Hydrogen movement into and out of fluid inclusions in quartz: Experimental evidence and geological implications, *Geochim. Cosmochim. Acta*, *58*, 141–148.

Ménez, B., P. Philippot, M. Mosbah, M. Drakopoulos, and A. Snigirev (1999), Fluid inclusion depth and thickness estimates using a Na nuclear reaction resonance and Si elastic scattering, *Nucl. Instrum. Methods Phys. Res., Sect. B*, *158*, 533–537.

Moss, R., and S. D. Scott (2001), Geochemistry and mineralogy of gold-rich hydrothermal precipitates from eastern Manus Basin, Papua New Guinea, *Can. Mineral.*, *39*, 957–978.

Mottl, M. J., , E. E. Davis, A. T. Fisher, and J. F. Slack (Eds.) (1994), *Proceedings of the Ocean Drilling Program*, *Scientific Results*, vol. 139, Ocean Drill. Program, College Station, Tex.

Parr, J. M., R. A. Binns, and J. B. Gemmell (1996), Sulfide chimneys from the Satanic Mills site in the PACMANUS hydrothermal field, Eastern Manus Basin, Papua New Guinea, *Eos Trans. AGU*, *77*, West. Pac. Geophys. Meet. Suppl., W120.

Paulick, H., D. A. Vanko, and C. J. Yeats (2004), Drill core-based facies reconstruction of a deep-marine, felsic volcano hosting an active hydrothermal system (Pual Ridge, Papua New Guinea, ODP Leg 193), *J. Volcanol. Geotherm. Res.*, doi:10.1016/S0377-0273(03)00275-0, *130*, 31–50.

Petersen, S., P. M. Herzig, and M. D. Hannington (1998), Fluid inclusion studies as a guide to the temperature regime within the TAG hydrothermal mound, 26°N, Mid-Atlantic Ridge, *Proc. Ocean Drill. Program Sci. Results*, *158*, 163–178.

Rimstidt, J. D. (1997), Gangue mineral transport and deposition, in *Geochemistry of Hydrothermal Ore Deposits*, edited by H. L. Barnes, 3rd ed., pp. 487–515, John Wiley, Hoboken, N. J.

Roberts, S., et al. (2003), Contrasting evolution of hydrothermal fluids in the PACMANUS system, Manus Basin: The Sr and S isotope evidence, *Geology*, *31*, 805–808.

Roedder, E. (1984), *Fluid Inclusions. Rev. Mineral.*, vol. 12, 664 pp., Mineral. Soc. of Am., Washington, D. C.

Ryan, C. G., C. A. Heinrich, E. van Achterbergh, C. Ballhaus, and T. P. Mernagh (1995), Microanalysis of ore-forming fluids using the scanning proton microprobe, *Nucl. Instrum. Methods Phys. Res., Sect. B*, *104*, 182–190.

Scott, S. D. (1997), Seafloor hydrothermal systems and deposits, in *Geochemistry of Hydrothermal Ore Deposits*, 3rd ed., edited by H. L. Barnes, Chapter 16, 797–875, John Wiley, Hoboken, N. J.

Scott, S. D., and R. A. Binns (1995), Hydrothermal processes and contrasting styles of mineralization in the western Woodlark and eastern Manus basins of the western Pacific, in *Hydrothermal Vents and Processes*, edited by L. M. Parson, C. L. Walker, and D. R. Dixon, *Geol. Soc. Spec. Publ.*, *87*, 191–205.

Shitashima, K., T. Gamo, K. Okamura, and J. Ishibashi (1997), Trace elements at the Manus Basin, Papua New Guinea, *JAMSTEC J. Deep Sea Res.*, *13*, 249–255.

Sinton, J. M., L. L. Ford, B. Chappell, and M. T. McCulloch (2003), Magma genesis and mantle heterogeneity in the Manus back-arc basin, Papua New Guinea, *J. Petrol.*, *44*, 159–195.

Taylor, B. J., K. A. W. Crook, and J. Sinton (1994), Extensional transform zones and oblique spreading centers, *J. Geophys. Res.*, *99*, 19,707–19,718.

Teagle, D. A. H., J. C. Alt, H. Chiba, and A. N. Halliday (1998), Dissecting an active hydrothermal deposit: The strontium and oxygen isotopic anatomy of the TAG hydrothermal mound-anhydrite, *Proc. Ocean Drill. Program Sci. Results*, *158*, 129–142.

Tivey, M. K., R. A. Mills, and D. A. H. Teagle (1998), Temperature and salinity of fluid inclusions in anhydrite as indicators of seawater entrainment and heating in the TAG active mound, *Proc. Ocean Drill. Program Sci. Results*, *158*, 179–190.

Vanko, D. A., M. Bonnin-Mosbah, P. Philippot, E. Roedder, and S. R. Sutton (2001), Fluid inclusions in quartz from oceanic hydrothermal specimens and the Bingham, Utah, porphyry-Cu deposit: A study with PIXE and SXRF, *Chem. Geol.*, *173*, 227–238.

Von Damm, K. L. (1995), Controls on the chemistry and temporal variability of seafloor hydrothermal fluids, in *Seafloor Hydrothermal Systems, Physical, Chemical, Biological and Geological Interactions*, *Geophys. Monogr. Ser.*, vol. 91, edited by S. E. Humphris et al., pp. 222–247, AGU, Washington, D. C.

Von Damm, K. L., L. G. Buttermore, S. E. Ooosting, A. M. Bray, D. J. Fornari, M. D. Lilley, and W. C. Shanks III (1997), Direct observation of the evolution of a seafloor 'black smoker' from vapor to brine, *Earth Planet. Sci. Lett.*, *149*, 101–112.

Von Damm, K. L., M. D. Lilley, W. C. Shanks III, M. Brockington, A. M. Bray, K. M. O'Grady, E. Olson, A. Graham, G. Proskurowski, and the SouEPR Science Party (2003), Extraordinary phase separation and segregation in vent fluids from the southern East Pacific Rise, *Earth Planet. Sci. Lett.*, *206*, 365–378.

Zhang, Y. G., and J. D. Franz (1987), Determination of the homogenization temperatures and densities of supercritical fluids in the system NaCl-KCl-$CaCl_2$-H_2O using synthetic fluid inclusions, *Chem. Geol.*, *64*, 335–350.

Zierenberg, R. A., et al. (1998), The deep structure of a sea-floor hydrothermal deposit, *Nature*, *392*, 485–488.

Zierenberg, R. A., Y. Fouquet, D. J. Miller, and W. Normark (Eds.) (2000), *Proceedings of the Ocean Drilling Program*, *Scientific Results*, vol. 169, Ocean Drill. Program, College Station, Tex.

W. Bach, Department of Marine Chemistry and Geochemistry, Woods Hole Oceanographic Institution, 360 Woods Hole Road, MS 8,Woods Hole, MA 02543, USA. (wbach@whoi.edu)

S. Roberts, School of Ocean and Earth Science, Southampton Oceanography Centre, University of Southampton, Southampton, SO14 3ZH, UK. (sr1@mail.soc.soton.ac.uk)

S. D. Scott, Department of Geology, University of Toronto, 22 Russell Street, Toronto, Ontario, Canada M5S 3B1. (scottsd@geology.utoronto.ca)

D. A. Vanko, Department of Physics, Astronomy and Geosciences, Towson University, 8000 York Road, Towson, MD 21252, USA. (dvanko@towson.edu)

C. J. Yeats, CSIRO Exploration and Mining, P.O. Box 136, North Ryde, New South Wales 1670, Australia.